Confinement and Chiral Symmetry in the $SU(3)$ Instanton-dyon Ensemble

Dallas DeMartini

Center for Nuclear Theory, Department of Physics and Astronomy,
Stony Brook University, Stony Brook, NY 11794-3800, USA

E-mail: dallas.demartini@stonybrook.edu

Confinement and chiral symmetry breaking remain two the most interesting and challenging nonperturbative phenomena in non-Abelian gauge theories. Recent semiclassical (for $SU(2)$) and lattice (for QCD) studies have suggested that confinement arises from interactions of statistical ensembles of instanton dyons with the Polyakov loop. In this proceeding, recent work is presented which has extended the study of semiclassical ensemble of dyons to the $SU(3)$ Yang-Mills theories with $N_f = 0$ and $N_f = 2$ flavors of massless, dynamical quarks. Dynamical quarks are included via the interaction of their topological zero modes on the dyons. It will be shown that such interactions do generate the expected first-order deconfinement phase transition in the $N_f = 0$ case and are compatible with a second-order transition in the $N_f = 2$ case. Studying the Dirac eigenvalue spectrum at multiple system sizes reveals that the overlap of the quark zero modes generates a nonzero condensate below T_c, breaking chiral symmetry.

PoS(LATTICE2021)175

1. Introduction

This talk was based on the work in Refs. [1, 2]. In this work it is shown how a semiclassical model of the dyons can generate both confinement (for both $N_f = 0, 2$) and chiral symmetry breaking (for only $N_f = 2$). Monte-Carlo simulations are performed with $O(100)$ dyons and antidyons, minimizing the free energy and determining the physical properties of the ensemble over a range of temperatures near T_c. While these phase transitions are well documented on the lattice, this work provides insight into the mechanisms that drive them by considering only a small fraction of the total degrees of freedom found in lattice simulations.

The dyons are dependent on the Polyakov loop which is the order parameter of the deconfinement phase transition, and drive the system to the confining phase via their nonperturbative interactions, which for high enough densities overcome the (deconfinement-favoring) perturbative interactions of thermal gluons. Additionally, dyons support topological quark zero modes. The overlap of these zero modes generates a spectrum of near-zero eigenvalues of the Dirac operator which gives rise to a nonzero quark condensate below some T_c and a nonzero eigenvalue gap above. The behavior of this spectrum has nontrivial volume dependence, so ensembles of different sizes are studied in order to extrapolate to the thermodynamic limit.

2. Instanton Dyons, Holonomy, and the Interactions

2.1 Dyons and holonomy

The instanton dyons (also known as instanton monopoles), discovered by Kraan, van Baal, Lee, and Lu [3, 4], are the constituent topological objects of the instanton that emerge when generalized to the case of a nonzero vacuum expectation value (VEV) of the Euclidean time component of the gauge field $\langle A_4^3 \rangle \neq 0$, also known as a nontrivial holonomy. In the $SU(3)$ theories considered here, there are three types of dyons M_1, M_2, and L, as well as corresponding antidyons, making for six species in total. The VEV of one component of the gauge field defines the holonomy v via $\langle A_4 \rangle = 2\pi T v$, which defines the dyons actions and sizes. The holonomy is related to the Polyakov loop by

$$\langle P \rangle = \frac{1}{3} + \frac{2}{3}\cos(2\pi v). \tag{1}$$

The (anti)dyons are both electrically- and magnetically-charged objects with (anti)self-dual fields. They also carry a fraction of the instanton action $S_0 = 8\pi^2/g^2$ and topological charge $Q = \pm 1$, proportional to their individual holonomies, $v_{M1} = v_{M2} = v$, and $v_L = 1 - 2v$. The semiclassical description of the dyons is reliant on the fact that the individual dyon actions $S_i = S_0 v_i$ are $\sim 3 - 4$ in the temperature range of interest.

The central aim of this work was to then compute the free energy of an interacting ensemble of dyons over a range of parameters (temperature T, holonomy v, and both dyon densities n_M, n_L) and determine the parameters that minimize it for each temperature. The free energy density computed

was given by

$$f(T, v, n_M, n_L) = -N_f \frac{4\pi^2}{3}(2v^4 - v^2) + \frac{4\pi^2}{3}(2(v(1-v))^2 + (2v(1-2v))^2)$$
$$- 4n_M \ln\left[\frac{d_v e}{n_M}\right] - 2n_L \ln\left[\frac{d_{1-2v} e}{n_L}\right] + \frac{\ln(8\pi^3 N_M^2 N_L)}{\tilde{V}_3} + \Delta f. \tag{2}$$

The first two terms are the perturbative holonomy potentials of the thermal quarks and gluons, respectively. The next three terms come from the dyon entropy, expanded to three terms with Sterling's approximation, where d_v is the quantum weight of a dyon with holonomy v [5]. The last term, Δf, is the free energy density contribution from the dyon interactions. It is the portion computed via Monte-Carlo integration over the dyons' collective coordinates.

The interaction-induced free energy is computed by standard integration over a dummy parameter

$$\Delta F = \int_0^1 \langle \Delta S(\lambda) \rangle d\lambda. \tag{3}$$

Integration over λ is done in 10 equal steps with $\lambda = 0.1, \ldots 1$. For every set of input parameters, 2000 configurations are sampled and averaged over at each value of λ. Each simulation is performed in a 3D box surrounded by 26 image boxes to enforce periodic boundary conditions. The interactions are broken into three conceptually-distinct parts: the classical-level binary interactions ΔS_{class}, the interactions from the one-loop correction to the metric G for dyons and $\bar{G}$ for antidyons, and the interactions from the fermionic determinant $\hat{T}$,

$$\Delta S = \Delta S_{class} - \ln(\det G \det \bar{G}) - N_f \ln(\det \hat{T}). \tag{4}$$

2.2 Dyon interactions

The instanton being a minimum of the action means that its constituent dyons do not experience a classical-level interaction with each other. Dyons and antidyons do however experience classical interactions with a parameterized form

$$\Delta S_{class}^{d\bar{d}} = -\frac{S_0 C_{d\bar{d}}}{2\pi}\left(\frac{1}{rT} - 2.75\pi\sqrt{v_i v_j}e^{-1.408\pi\sqrt{v_i v_j}rT}\right), \tag{5}$$

where $C_{d\bar{d}}$ is a coefficient with value 2 for pairs of the same type and -1 for pairs of different types. These interactions are used for distances greater than the core size $r_0 = x_0/(2\pi v T)$. Dyons pairs of the same type (regardless of duality) experience a repulsive core at short ranges. While the core potential has not been studied in detail, it is reasonably described by

$$\Delta S_{class}^{core} = \frac{v_i V_0}{1 + e^{2\pi v_i T(r-r_0)}}. \tag{6}$$

Additionally, the dyons experience an effective potential from the fluctuation determinant of the instanton. This effect leads to the so-called Diakonov determinant of the metric of the space of dyons' collective variables

$$G_{im,jn} = \delta_{ij}\delta_{mn}\left(4\pi v_m - \sum_{k\neq i}\frac{2}{T|r_{i,m} - r_{k,m}|} + \sum_k \frac{1}{T|r_{i,m} - r_{k,p\neq m}|}\right)$$
$$+ \frac{2\delta_{mn}}{T|r_{i,m} - r_{j,n}|} - \frac{1 - \delta_{mn}}{T|r_{i,m} - r_{j,n}|}, \tag{7}$$

where $r_{i,m}$ is the position of the i'th dyon of type m. This metric only accounts for the selfdual dyons. An equivalent metric $\bar{G}$ is used for the antidyons as well. All of the long range terms in the interactions are regulated by a Debye screening mass $r \to re^{M_D rT}$. This mass, along with the core parameters V_0 and x_0 are not known from first principles and are instead phenomenological choices. The values of these parameters are different between the $N_f = 0$ and $N_f = 2$ cases (the theories have different runnings of the coupling and thus, different scales). In the absence of first-principles derivations, their values should be constrained to improve agreement with lattice information on the dyons, such as the dyon densities and correlations.

2.3 Fermionic determinant

Dynamical quarks are included via the fermionic determinant. The fermionic determinant is included in the dyon model by considering only the subspace spanned by the quark zero modes. This results in the so-called 'hopping matrix' $\hat{T}$. The hopping matrix has the simple form for massless quarks

$$\hat{T} = \begin{pmatrix} 0 & T_{ij} \\ -T_{ji} & 0 \end{pmatrix}, \tag{8}$$

where T_{ij} is the overlap of the right-handed zero mode on L-dyon i and the left-handed zero mode on $\bar{L}$-antidyon j. This overlap element, in general, requires intricate numerical integration and is parameterized by

$$T_{ij} = \bar{\nu}c' \exp(-\sqrt{11.2 + (\pi\bar{\nu}rT)^2}). \tag{9}$$

The fermionic determinant $\det(\hat{T})$ represents the set of diagrams of closed loops of quarks hopping between dyons and antidyons. When the determinant is dominated by short hopping loops involving just two dyons, the ensemble has only large eigenvalues and chiral symmetry is restored. When the ensemble is dense and there are collectivized modes involving many dyons, eigenvalues near zero appear breaking chiral symmetry. While not discussed in this talk, nonzero quark mass can be included by adding quark mass terms on the diagonals of the hopping matrix, giving rise to more loop diagrams.

3. Polyakov Loop and Confinement for $N_f = 0, 2$

The dyon densities and average Polyakov loop of the ensembles are determined by the location of the free energy density minima. The dyon densities are sensitive to the breaking of center symmetry in the theories. In the pure gauge theory, $\mathbb{Z}_3$ symmetry is restored in the confined phase, making all dyon densities equal as shown in Fig. 1. When quarks are included, this symmetry is broken at all temperatures, meaning that the dyons have unequal densities, even when their actions and sizes are all equal. In other words, the inclusion of the quark-induced potential between L and $\bar{L}$ dyons suppresses their density.

The structure of the holonomy potential itself gives some insight into the physics near the phase transition. For the pure gauge theory, close to T_c, both above and below, two distinct free energy minima can be observed as in Fig. 2. One minima, which is the global minimum below T_c lies at the confining holonomy, while the other at a nonzero value of $\langle P \rangle$. In the two-flavor case, only one minimum is seen, with its location smoothly varying as a function of temperature.

4
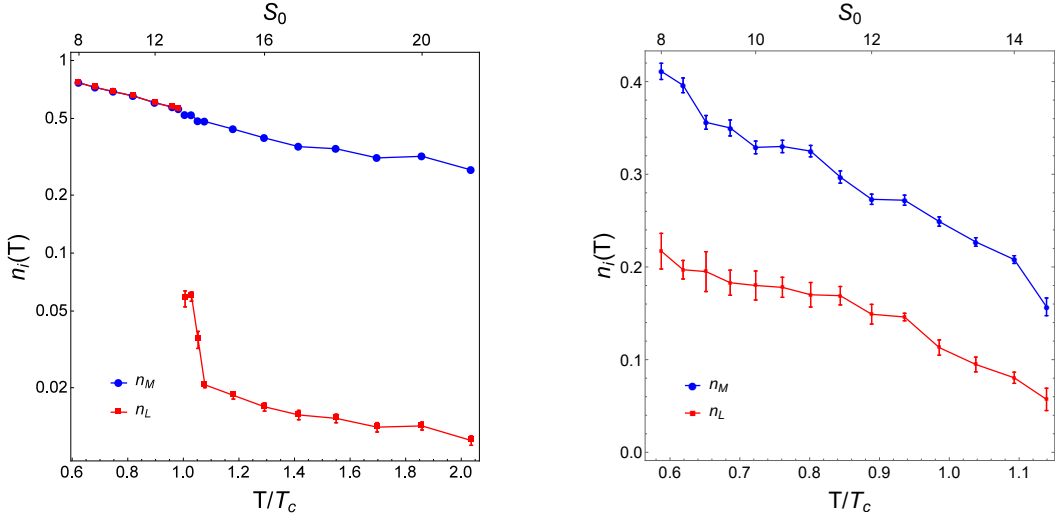
Figure 1: Dyon densities as functions of temperature for both $N_f = 0$ (left) and $N_f = 2$ (right).
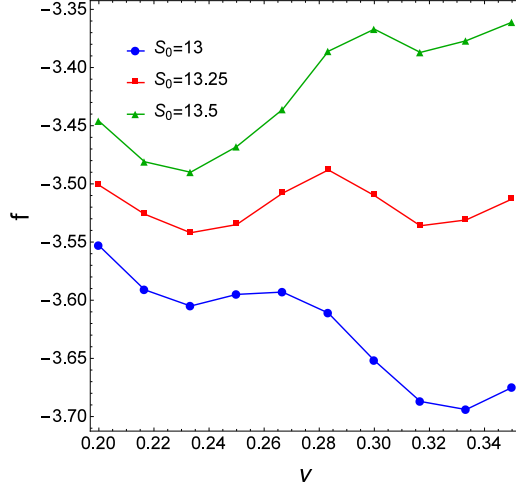
Figure 2: Holonomy dependence of the minimum free energy density near the phase transition for $N_f = 0$.

In the pure $SU(3)$ case, the dyons display the well-known first order deconfinement phase transition with the Polyakov loop jumping from 0 to ~ 0.4 as seen on the lattice [6]. In the case with two flavors, the transition is now smooth. The free energy, and thus Polyakov loop, behave as 'energy-like' operators in the effective Hamiltonian near the phase transition. The deconfinement transition in the massless $N_f = 2$ theory is expected to be a second-order transition belonging to the 3D $O(4)$ universality class (or $O(2)$ in the case of finite lattice spacing, as seen in e.g. Ref. [7]).

To determine the deconfinement temperature T_{deconf}, $\langle P(T) \rangle$ is fit to the form

$$\langle P(T) \rangle = \exp \left(- a_0 - t(a_1 + A|t|^{-\alpha}) \right), \tag{10}$$

where $t = (T - T_{deconf})/T_{deconf}$ and $\alpha = 2 - \beta(1 + \delta)$ is the hyperscaling variable with the values of the $O(4)$ class $\beta = 0.380$, $\delta = 4.824$, and $\alpha = -0.2131$. The dyon data shows reasonable agreement with the form expected in the $O(4)$ universality class, suggesting a second-

order transition. (Note that in the plots T_c refers to the deconfinement temperature when $N_f = 0$ and the chiral restoration temperature when $N_f = 2$.)
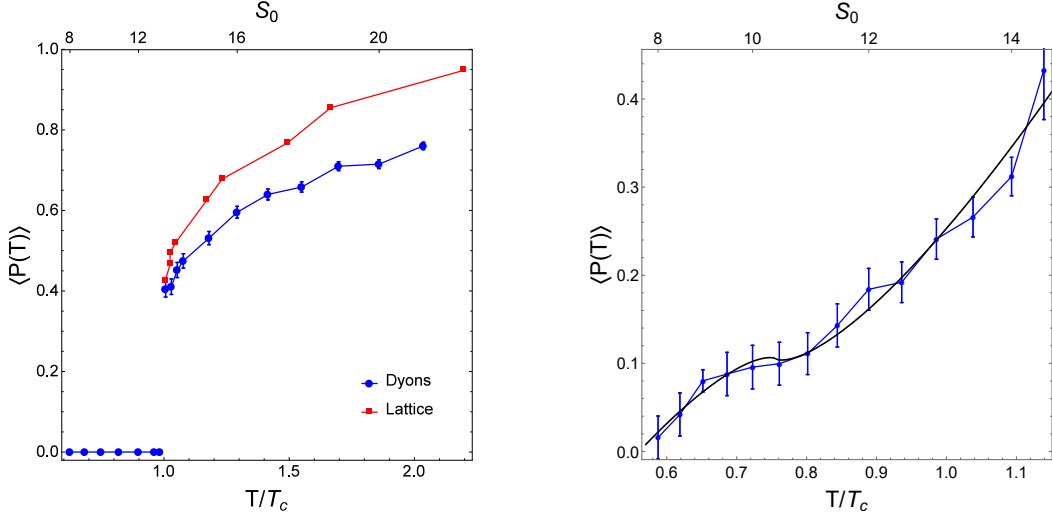
Figure 3: Average Polyakov loop as a function of the temperature for $N_f = 0$ (left) and $N_f = 2$ (right). Lattice data in the left figure is taken from Ref. [6]. Solid curve in the right figure is a fit to the form expected in the 3D $O(4)$ universality class.

4. Dirac Eigenvalue Spectrum and Chiral Symmetry for $N_f = 2$

4.1 Dirac eigenvalue spectrum

In the limit of massless quarks, QCD-like theories have a chiral flavor symmetry $SU(N_f)_L \times SU(N_f)_R$ that is spontaneously broken below some T_c. The order parameter for this symmetry is the quark condensate $\langle \bar{q}q \rangle$, which is nonzero in the broken phase. This condensate is obtained by studying the near-zero-mode zone of the Dirac eigenvalues, which are related to the condensate via the Banks-Casher relation [8]

$$\Sigma = |\langle \bar{q}q \rangle| = \lim_{\lambda \to 0} \lim_{V \to \infty} \pi \rho(\lambda). \tag{11}$$

Examples of the eigenvalue distributions of both phases are shown in Fig. 4. The distributions shown are done at $N_D \simeq 120$. Both distributions show an absence of eigenvalues nearest to zero; in the broken phase this is a finite-volume effect and in the restored phase this is a physical disappearance of near-zero modes. To see this, one must take the infinite-volume limit by performing multiple simulations with different ensemble volumes.

4.2 Infinite-volume extrapolation and results

Extrapolation to infinite volume is done by running simulations at three different numbers of dyons $N_D \simeq 120, 240, 360$ for each temperature studied. In order to determine which phase the system is in, two different methods are used to look at two different observables. The first is the
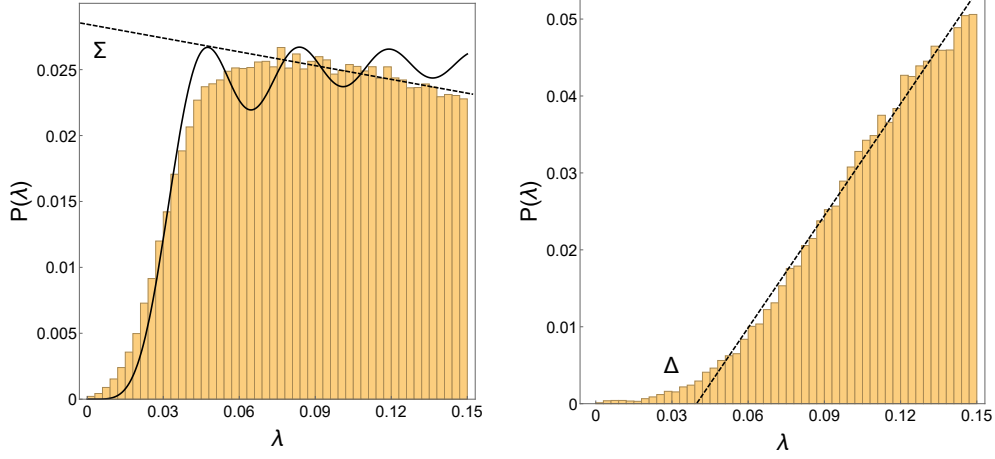
Figure 4: Normalized probability distribution of eigenvalues in the near-zero-mode zone for both the broken and restored phases. Dashed lines show fits to the linear regions of the distributions. Left: $S_0 = 8$, the y-intercept of the fit is proportional to the chiral condensate Σ, the solid curve is the fit to the random-matrix theory results (12), Right: $S_0 = 14$, the x-intercept of the fit is the eigenvalue gap Δ. Note that the linear fit to determine the y-intercept on the left plot is not used in the analysis and is merely illustrative.

chiral condensate. For each of the three sizes, the lowest eigenvalues (where the distribution falls quickly near zero) are fit to results from random-matrix theory [9] (see Fig. 4 (left))

$$\rho(z) = V\Sigma_2 \left(\frac{z}{2} (J_2^2(z) - J_1(z)J_3(z)) \right), \tag{12}$$

where $z = \lambda V\Sigma_1$ and J_n are the Bessel functions. Each of the sizes gives two fit parameters, Σ_1 and Σ_2, the former being volume dependent and the latter being volume independent. An interpolating function is used to relate the parameters from different system sizes to extract the infinite-volume condensate.

In addition to the condensate that disappears above T_c, the distributions should develop a nonzero eigenvalue gap $\Delta(T)$, below which no eigenvalues are seen, above T_c. At each ensemble size, the approximately-linear region of the distribution is fit to a linear function and the x-intercept is the eigenvalue gap (see Fig. 4 (right)). The three gaps are then fit a linear function in $1/V$ and the value at $1/V = 0$ is the physical gap that remains when finite-volume effects are removed. Results for both of these observables are shown in Fig. 5.

The chiral phase transition is sensitive to the light quark masses. Recent lattice studies have found that reducing the up and down quark masses by just a few MeV from their physical values reduces the critical temperature by more than 20 MeV [10]. Also, the order of the chiral phase transition is sensitive as well. Like the deconfinement transition, it is expected to be second order, belonging to the same $O(4)$ class. Near T_c, the condensate is expected to behave as

$$\Sigma(T) = \begin{cases} C(T_c - T)^\beta & \text{if } T < T_c \\ 0 & \text{if } T \geq T_c \end{cases} \tag{13}$$

7
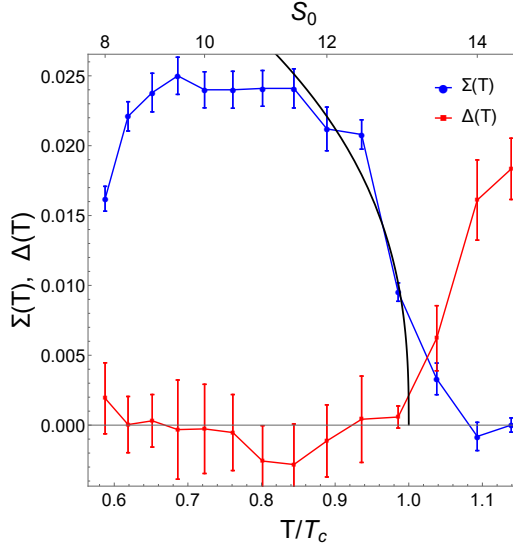
Figure 5: The chiral quark condensate $\Sigma(T)$ and the eigenvalue gap $\Delta(T)$ as functions of the temperature. Solid curve is the form of the condensate from the $O(4)$ universality class (13) and is a fit to the four data points just below T_c. The overall normalization of $\Sigma(T)$ is arbitrary.

The location of T_c is determined from a fit to this function to the points just below T_c. Both the condensate $\Sigma(T)$ and eigenvalue gap $\Delta(T)$ change rapidly almost simultaneously, providing a consistent determination of the critical temperature.

5. Summary

Numerical simulations of $O(100)$ instanton dyons in the $SU(3)$ gauge group with and without dynamical quarks were performed in order to study the role of the dyons in the deconfinement and chiral symmetry phase transitions. The properties of the dyon ensembles were determined on both sides of the phase transitions.

The results suggest that confinement and chiral symmetry breaking may both be explained by the non-perturbative interactions of a high density ensemble of dyons. As the temperature is decreased, the dyon interactions deform the holonomy potential and drive the system to the confined phase while the collective overlap of dense quark zero modes spontaneously break chiral symmetry. Each of the phase transitions show behavior consistent with what has been observed on the lattice.

Acknowledgments

References

[1] D. DeMartini and E. Shuryak, *Deconfinement phase transition in the SU(3) instanton-dyon ensemble*, *Phys. Rev. D* **104**, no.5, 054010 (2021).

[2] D. DeMartini and E. Shuryak, *Chiral Symmetry Breaking and Confinement from an Interacting Ensemble of Instanton-dyons in Two-flavor Massless QCD*, 2108.06353 [hep-ph].

[3] T. C. Kraan and P. van Baal, *Monopole constituents inside SU(n) calorons*, *Phys. Lett. B* **435**, 389-395 (1998).

[4] K. M. Lee and C. h. Lu, *SU(2) calorons and magnetic monopoles*, *Phys. Rev. D* **58**, 025011 (1998).

[5] D. Diakonov, N. Gromov, V. Petrov and S. Slizovskiy, *Quantum weights of dyons and of instantons with nontrivial holonomy*, *Phys. Rev. D* **70**, 036003 (2004).

[6] O. Kaczmarek, F. Karsch, P. Petreczky and F. Zantow, *Heavy quark anti-quark free energy and the renormalized Polyakov loop*, *Phys. Lett. B* **543**, 41-47 (2002).

[7] D. A. Clarke, O. Kaczmarek, F. Karsch, A. Lahiri and M. Sarkar, *Sensitivity of the Polyakov loop and related observables to chiral symmetry restoration*, *Phys. Rev. D* **103**, no.1, L011501 (2021).

[8] T. Banks and A. Casher, *Chiral Symmetry Breaking in Confining Theories*, *Nucl. Phys. B* **169**, 103-125 (1980).

[9] J. J. M. Verbaarschot and I. Zahed, *Spectral density of the QCD Dirac operator near zero virtuality*, *Phys. Rev. Lett.* **70**, 3852-3855 (1993).

[10] H. T. Ding *et al.* [HotQCD], *Chiral Phase Transition Temperature in (2+1)-Flavor QCD*, *Phys. Rev. Lett.* **123**, no.6, 062002 (2019).